

# EVALUATION OF TROPICAL CYCLONE GENESIS PRECURSORS WITH RELATIVE OPERATING CHARACTERISTICS (ROC) IN HIGH-RESOLUTION ENSEMBLE FORECASTS: HURRICANE ERNESTO

LEVI THATCHER AND ZHAOXIA PU\*

*Department of Atmospheric Sciences, University of Utah, Salt Lake City, Utah, U.S.A.*

## ABSTRACT

Identifying the environmental conditions that control tropical cyclone (TC) genesis is a challenging problem. This study examines a new method to evaluate the precursors of TC genesis using high-resolution ensemble forecasts and relative operating characteristic (ROC) diagrams.

With an advanced research version of the Weather Research and Forecasting (WRF) model, high-resolution ensemble forecasts (at 5 km horizontal resolution) are conducted in various configurations using a bred vector method to form a set of 140 ensemble members for predicting Hurricane Ernesto's genesis. Basic evaluation shows that high-resolution ensemble forecasts are able to predict well-developed TCs, whereas the NCEP Global Ensemble Forecast System (GEFS) fails to do so. This set of 140 ensemble members is employed to study the precursors of Hurricane Ernesto's genesis by contrasting the genesis and nongenesis cases. Specifically, ROC curves, composite figures for genesis and nongenesis cases, and Kolmogorov-Smirnov tests are applied to characterize the relationship between important environmental parameters near the beginning of the simulation and genesis likelihood 15–18 h later. It is found that moist conditions at 850 hPa, vertical wind shear, the strength of the 850 hPa pre existing wave, and upper-level warming play notable roles in Ernesto's genesis.

*Keywords:* tropical cyclone genesis, ensemble forecasting, relative operating characteristics, WRF, bred vector

## 1. Introduction

Of the many issues facing the weather prediction community in the last several decades, the challenges regarding tropical cyclone (TC) genesis stand out as some of the most vexing. Although significant improvements in track predictions have been achieved (Aberson 2001, Rogers et al. 2006, Gall et al. 2013), it is still very difficult to predict, one to several days in advance, the formation of a tropical cyclone (Hennon and Hobgood 2003; Kerns et al. 2008),

Several factors contribute to our limited ability to produce accurate forecasts of TC genesis: sparseness of observations over the oceans where the TC often form; a lack of understanding of the physical processes accompanying TC formation; and insufficient model resolution to explicitly resolve essential small-scale processes (Rogers et al. 2006). In order to address the data sparseness and deficiencies in numerical weather prediction models, ensemble forecasting has been developed and has become operational in many

major numerical weather prediction (NWP) centers around the world (e.g., Toth and Kalnay 1997; Buizza et al. 1999; Wei et al. 2008; Reynolds et al. 2008). Thus, many TC genesis-related studies have used global ensemble outputs (Cheung and Elsberry 2002; McLay et al. 2008; Snyder et al. 2010, 2011). In addition, many previous studies have focused on investigating the dynamic and physical processes that influence TC genesis. It has been well recognized that environmental conditions, such as sea-surface temperatures (SSTs), mid level moisture, upper-level divergence and warming, vertical shear, and low-level vorticity can all influence TC genesis (Gray 1968; McBride and Zehr 1981; Chen and Frank 1993; Bister and Emanuel 1997; Ritchie and Holland 1997; Simpson et al. 1997; Montgomery and Enagonio 1998; Zhang and Zhu 2012).

One of the key questions is whether a surface-concentrated (warm-core) tropical depression vortex results from a midlevel mesocyclone or whether it originates closer to the ocean surface. Reasor et al. (2005) affirmed that the establishment of this surface vortex is central to TC genesis. Bister and Emanuel (1997) used an axisymmetric, nonhydrostatic model to investigate how a midlevel mesoscale

---

*Corresponding author address:* Dr. Zhaoxia Pu, Department of Atmospheric Sciences, University of Utah, 135 S 1460 E, Rm 819, Salt Lake City, UT 84112, U.S.A. E-mail: Zhaoxia.Pu@utah.edu

vortex became a tropical depression during the formation of Hurricane Guillermo. They showed that the mesoscale vortex preceding Guillermo was initially found within the stratiform rain region of a Mesoscale Convective System (MCS). The downdrafts in this region, through the vertical advection of vorticity, helped build the surface vortex. Ritchie and Holland (1997) and Simpson et al. (1997), in their respective studies of Typhoon Irving and TC Oliver, also found that midlevel vortices play an integral role in the formation of warm-core, surface-concentrated tropical depressions.

Other researchers believe that mechanisms associated with genesis evolve through more of a “bottom-up pathway” (Montgomery et al. 2010). For example, Montgomery and Enagonio (1998) showed that vortex intensification proceeds as low-level vorticity, which is generated by mesoscale convective vortex-related convective bursts, and can spin up a surface-circulation through horizontal axisymmetrization. Similarly, Davis and Bosart (2001) found that genesis-related potential vorticity (PV) anomalies began in the lower levels in Hurricane Diana (1984). Later, Hendricks et al. (2004) found that the most important influence on Diana’s genesis was “small-scale cores of deep cumulonimbus convection that form in a vorticity-rich environment.” Reasor et al. (2005) and Montgomery et al. (2006) subsequently clarified the role of cumulonimbus and vortical hot towers (VHTs) in converging vorticity and triggering tropical cyclogenesis. More recently, Dunkerton et al. (2009) and Montgomery et al. (2010) refined their explanation of the development process in proposing their marsupial pouch theory of TC genesis. In these papers, a “Kelvin cat’s eye,” or protective pouch, is thought to be necessary for TC genesis because it provides a region of cyclonic vorticity, weak deformation, moisture containment, and maintenance of the parent (easterly) wave until the “developing proto-vortex becomes a self-sustaining entity and emerges from the wave as a tropical depression” (Montgomery et al. 2010).

Recent modeling studies have looked at the effects of instability, moisture, and vertical motion on TC genesis and have found the mechanisms to be less straightforward. For example, Nolan et al. (2007) used a radiative-convective equilibrium model to investigate the sensitivity of a numerical simulation of TC genesis to environmental parameters and found no relationship between moisture-dependent convective available potential energy (CAPE) and the rate of cyclone development. Sippel and Zhang (2008) used a set of ensemble forecasts from the Penn State University/National Center for Atmospheric Research (NCAR) Mesoscale Model Version 5 (MM5) to investigate the predictability of cyclogenesis by examining a disturbance in the Gulf of Mexico. Contrary to Nolan et al. (2007), they found that the two most important parameters for genesis were deep moisture and CAPE. These findings closely tie in to the role of downdrafts in TC genesis. If enough moisture

is not present in the midtroposphere, then convection has the propensity to produce cold downdrafts and stabilize the lower troposphere (Sippel and Zhang 2008). Bister and Emanuel (1997) similarly emphasized the importance of moisture, but hypothesized that a low-level cold core could cause genesis by increasing the important updraft-to-downdraft ratio.

In light of the continuing uncertainty regarding the effect of moisture and pre-existing vorticity on TC genesis, the relationship between these precursors and subsequent storm formation still needs to be evaluated. In order to better understand the role of these important environmental precursors, it is necessary to statistically characterize and compare them in developing versus nondeveloping cases. In this study, we aim to use a set of high-resolution regional ensemble forecasts to evaluate the effects of environmental precursors on TC genesis.

As mentioned, ensemble forecasting can overcome the initial condition errors in NWP by producing a set of forecasts with varying initial conditions. Therefore, instead of generating a single, or deterministic, forecast, it produces a set of multiple forecast members, assuming that the mean of these ensemble members provides the best forecast and that the spread of the ensemble members offers an estimate of the associated forecast uncertainties. Specifically, for TC genesis forecasting, ensemble forecasts could provide the probability of genesis in a set of forecasts. Through contrasts between the developing and nondeveloping tropical waves produced by ensemble forecasts for the same case, we expect to obtain some statistical insights into the factors (e.g., environmental precursors) that influence TC genesis.

Specifically, in this study we will use a mesoscale community Weather Research and Forecasting (WRF) model (Skamarock et al. 2008) to generate a set of regional ensemble forecasts for the genesis of Hurricane Ernesto (2006). We will then use relative operating characteristics (ROC) diagrams to characterize the relationship between important environmental parameters and TC genesis in order to determine key factors that could provide genesis predictive power.

Considering its wide usage, computational efficiency, and competitiveness over short forecast periods (as revealed in McLay et al. 2008; see their Figure 2), in this study we will use a bred vector scheme (Toth and Kalnay 1993, 1997) to generate ensemble perturbations for a large number of model initial states in a pregenesis environment of Hurricane Ernesto. Owing to the objective of examining TC environmental precursors, the ensemble experiments will be performed only with perturbed initial conditions. The advantage of using the high-resolution (~5 km) regional ensemble is to increase genesis predictability and thus create a set of ensembles with good sample sizes of developing and nondeveloping cases.

The specific questions regarding the TC genesis to be addressed in this paper include: 1) What are the most im-

portant environmental precursors to Hurricane Ernesto's genesis? 2) At what level does water vapor most promote genesis? 3) Does vertical shear play a more important role than water vapor in genesis? 4) Do the ensemble forecasts suggest a bottom-up or top-down route to Ernesto's genesis?

The paper is organized as follows: Section 2 describes the model setup, experimental design, and configurations of the ensemble forecasts. Section 3 summarizes and evaluates the high-resolution ensemble forecast results. Section 4 introduces the relative operating characteristics (ROC) diagram. Section 5 evaluates the environmental precursors and genesis for Hurricane Ernesto using ROC in the ensemble forecasts. Finally, Section 6 summarizes the major findings and gives concluding remarks.

## 2. Description of the case, model, ensemble method and experiments

### a. A brief overview of Hurricane Ernesto

Although originating as a tropical wave off the coast of Africa, Hurricane Ernesto (2006) did not achieve any notable organization until an associated surface low developed as the disturbance approached the Lesser Antilles. Moving toward the northeast, the disturbance developed into a tropical depression (TD) at 1800 UTC 24 August 2006, roughly 40 nautical mi north-northwest of Grenada. Subsequently, the depression experienced increased convection over the low-level center as it moved north-northwest south of a ridge over the western Atlantic Ocean. At 1200 UTC 25 August 2006, the disturbance reached tropical storm (TS) status and turned to the northwest. Later, the storm reached hurricane status at 0600 UTC 27 August just south of Haiti. Then, Ernesto experienced several periods of strengthening and weakening, and eventually made landfall in Cuba, Florida, and North Carolina, according to the report from the National Hurricane Center (NHC).

Hurricane Ernesto (2006) is chosen as the primary focus of this study because 1) it caused significant damage in the US and Caribbean and 2) it has been documented as an especially difficult forecast for the NCEP Global Ensemble Forecast System (GEFS) (Snyder et al. 2010; Liu et al. 2012).

### b. WRF model and setup

An advanced research version of the WRF model (version 3.3.0) (Skamarock 2008) is used with three-level nested domains at 45km, 15 km and an inner-most resolution of 5 km. Details of the model domain configurations are given in Table 1. The location of the domains is shown in Figure 1. In the vertical, there are 36  $\sigma$  levels and the top is set at 50 hPa. The Purdue Lin scheme (Chen and Sun 2002) is used for the microphysics, the Yonsei University scheme (Hong et al. 2006) is used for the boundary layer parameterization, and the Grell-Devenyi cumulus scheme (Grell and Devenyi 2002) is used for the cumulus parameterization, but only in

**TABLE 1.** Dimensions, grid spaces, and time steps of domains for numerical forecasts

Domain	Dimension ( $x \times y \times z$ )	Grid space	Time step
1	$125 \times 70 \times 36$	45 km	120 s
2	$331 \times 148 \times 36$	15 km	40 s
3	$844 \times 340 \times 36$	5 km	13.3 s

the outer two domains (at 45km and 15 km grid spacings). In addition, the Dudhia (Dudhia 1989) and the rapid radiative transfer model schemes (Mlawer et al. 1997) are used for short and longwave radiation, respectively.

### c. Perturbation method and ensemble experiments

Following Cheung and Elsberry (2002) and Snyder et al. (2010), we define the genesis time as occurring when the NHC designated Ernesto a tropical depression at 1800 UTC 24 August 2006. In order to predict the genesis of Ernesto, forecast initial time is set at 0000 UTC 24 August 2006 and the ensemble forecasts are extended for 36 h until 1200 UTC 25 August 2006. The control ensemble forecast (CNTL, hereafter) is a set of regional ensemble forecasts using WRF, generated by downscaled initial conditions (ICs) from the NCEP GEFS with the boundary conditions (BCs) derived from NCEP Global Forecast System (GFS)  $1 \times 1^\circ$  final analysis (FNL) data in order to be consistent with other regional ensemble experiments in this study. Since GEFS has only 14 members in 2006 and since the computational cost of high-resolution ensemble forecasts is considerable, the WRF regional ensemble experiments will use 14 members to achieve consistent comparisons.

For regional ensemble forecasts with the bred vector method, the breeding period begins at 0000 UTC 23 August 2006 and the breeding cycles are performed, separately for different experiments, every 3, 6, and 12 h, ending at 0000 UTC 24 August 2006 (which is the initial time for the ensemble forecasts). In order to examine the effects of individual perturbed variables on resulting forecasts and also to increase the sample size of ensemble forecasts, in addition to perturbing four important variables at once (water vapor, potential temperature or  $\theta$  hereafter, and u and v components), experiments are also designed to perturb each individual variable separately and in various combinations. Water vapor here is defined as specific humidity ( $\text{g kg}^{-1}$ ).

The ensemble forecasts are created with the WRF model using a bred vector method. The analysis state is obtained by interpolating NCEPGEFS final analysis (at  $1^\circ \times 1^\circ$  resolution) down to WRF regional domains. At the beginning of the breeding cycle, WRF initial fields are derived from corresponding GEFS member ICs to obtain perturbed initial conditions. In the subsequent breeding cycles during the cycling period, perturbations are generated by performing the following for 14 members: 1) integrating the perturbed member for a predetermined cycle period (e.g., 3 h, 6 h

or 12 h); 2) differentiating, in terms of the chosen state variable(s) to be perturbed, the member's output compared to the analysis at the end of the cycle period to obtain the forecasted differences (projected error growth); 3) scaling down the forecasting differences so the magnitude of the mean difference matches the magnitude of the errors at the initial time (analysis errors); 4) adding the scaled perturbations to the analysis to obtain initial conditions (in terms of the specified variable) for ensemble members for the next cycle; and 5) integrating each member to the next cycle time and then repeating steps 1)-4).

The bred vector perturbation scheme used in this study is similar to a breeding of growing modes (BGM) setup constructed by McLay et al. (2008). A spatially invariant, or averaged, scaling factor is used to scale down the magnitude of forecast differences at the end of each cycle period to the size of initial analysis errors. Unlike many lower-

resolution BGM configurations (McLay et al. 2008; Wei et al., 2008), the scaled perturbations are added to the analysis only during the breeding cycle but are not subtracted at the same time to double the number of members. This is partially due to the consideration of the computational cost of additional ensemble members at high-resolution but it is also because Wei et al. (2008) indicated that adding and subtracting perturbations at the same time does not increase the effective degrees of freedom (EDF) of the ensemble.

Table 2 lists the configurations of all WRF-based regional ensemble experiments in this study. Except for CNTL, regional ensemble forecasts are performed to test 1) the effects of perturbing different variables (FNLq3, FNLth3, FNLuv3, FNLuvqt3); 2) the use of various cycling periods (FNLuvqt6 and FNLuvqt12 for the 6h and 12 h cycling period, respectively); 3) the boundary conditions (FNLuvqt3\_GEFSBCs is the same as FNLuvqt3 but uses the GEFS

**TABLE 2.** Configurations of all initial condition-based high-resolution regional ensemble forecasts

Ensemble experiment name	Variable perturbed	BCs	Breeding cycle period (h)	Variable scaling factor	Genesis probability
CNTL	from GEFS	FNL	N/A	N/A	7/14
FNLq3	Q	FNL	3	N	3/14
FNLth3	T	FNL	3	N	11/14
FNLuv3	U,V	FNL	3	N	12/14
FNLuvqt3	Q,T,U,V	FNL	3	N	4/14
FNLuvqt6	Q,T,U,V	FNL	6	N	3/14
FNLuvqt12	Q,T,U,V	FNL	12	N	3/14
FNLq3_height	Q	FNL	3	Y	1/14
FNLuvqt3_GEFSBCs	Q,T,U,V	GEFS	3	N	3/14
GEFSth3	T in GEFS	FNL	N/A	N	4/14

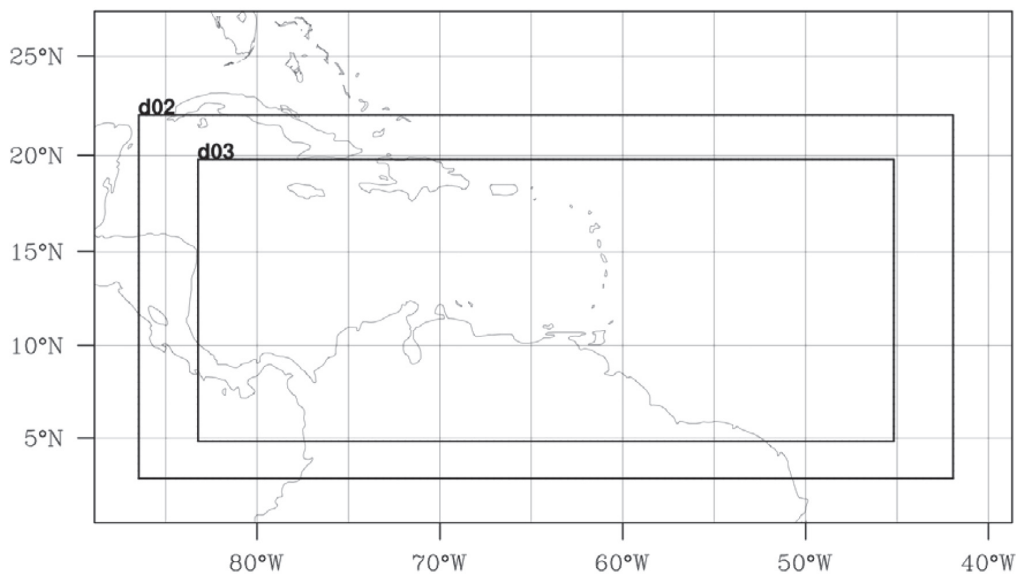


**FIG. 1.** WRF domains used for all ensemble simulations of Hurricane Ernesto.

boundary conditions instead of FNL) 4) the use of variable scaling factors at different heights (FNLq3\_height) and 5) the use of  $\theta$  perturbation in GEFS ICs (GEFSth3). With the various ensemble experiments, we expect not only to learn about the impacts of the above-mentioned factors on ensemble forecasts, but also to obtain a large enough sample size to determine, with statistical significance, the most important TC environmental precursors.

### 3. High-resolution ensemble forecast results and basic evaluation

#### a. Bias

We first evaluate the performance of regional ensemble forecasts by checking the time evolution of bias. The bias here represents the ensemble mean minus the corresponding analysis field, expressed as

$$\frac{1}{n} \sum_{k=1}^n (\bar{f}_k - a_k), \quad (1)$$

where  $\bar{f}$  denotes the ensemble mean of forecasts across the 14 ensemble members,  $a$  denotes the analysis,  $k$  denotes the

grid points across the domain, and  $n$  represents total grid points in the model domain.

Figure 2 displays a time series of bias at 850 hPa through the simulation period of 0000 UTC to 1800 UTC 24 August 2006 for both water vapor and  $\theta$  in various ensemble experiments. Notice that water vapor ( $\theta$ ) bias at this height generally remains within 0.5 g/kg (0.3 K). While the configurations of ensemble forecasts are significantly different from each other and the biases of the initial condition are different, over time the biases largely retain the same sign. In addition, the inter-ensemble initial vapor bifurcation is almost completely eliminated within several hours in the forecast period, indicating that initial perturbations generated by the bred vector method do not necessarily increase bias when integrating the model forward. Compared to the CNTL, which is downscaled from GEFS (large-scale ensemble), the bred ensembles perform quite favorably in terms of keeping the forecast bias within a reasonable range.

In order to better ascertain these bias differences with height, Figure 3 shows the averaged biases from 1200 to 1800 UTC for water vapor and  $\theta$ . Within 50 hPa from the surface, all ensemble forecasts show similar va-

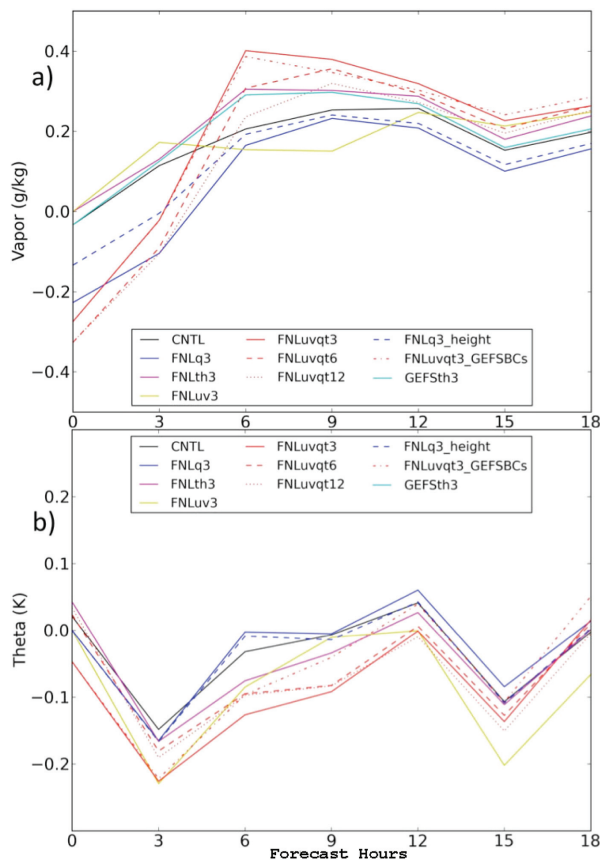


FIG. 2. Time series of bias at 850 hPa for selected ensembles for a) vapor (g/kg) and b) theta (K) between 0000 and 1800 UTC 24 August 2006.

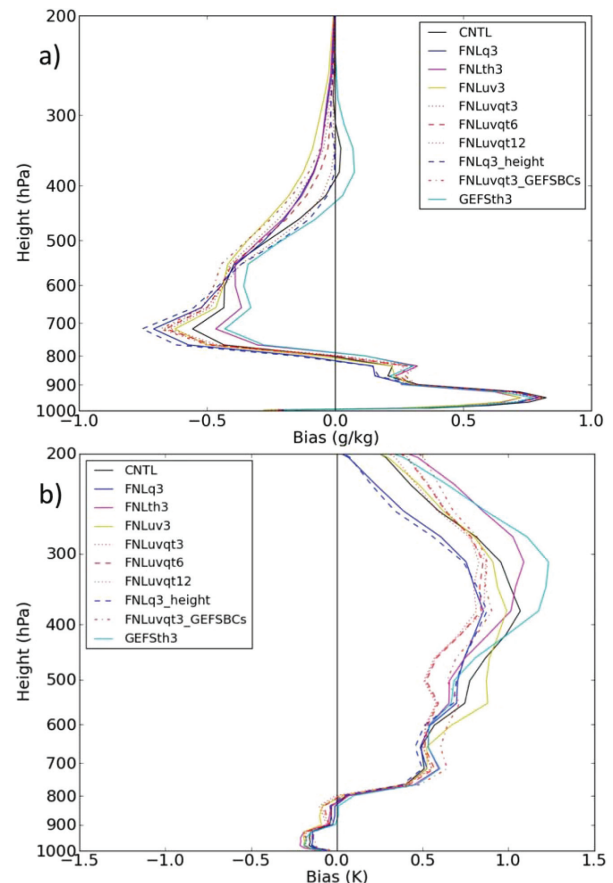


FIG. 3. Bias by height from 1200 to 1800 UTC for selected ensembles for a) vapor (g/kg) and b) theta (K).

por bias, which may be due to the use of the same surface parameterization schemes for all ensembles. Elsewhere, however, the various ensemble forecasts result in notable differences in the bias with height, primarily in terms of  $\theta$  values. For example, at most heights, the FNLuvqt3 show domain-averaged bias values 0.3 K less than those of the FNLuv3 in terms of  $\theta$ . While the vapor difference between ensembles is less, the least amount of vapor bias around 700 hPa is found in the FNLth3, which demonstrates that breeding a particular variable can cause notable differences not only in that variable itself (e.g.,  $\theta$ ), but also in those variables that interact with it (e.g., vapor). In general, the bias of the breeding ensembles is comparable to that of the CNTL.

#### *b. Predictability of Ernesto's genesis in regional ensemble forecasts*

In order to determine whether TC genesis occurs in a certain member of an ensemble forecast, there must be a closed 850 hPa geopotential contour of 1496 m or below and a maximum vorticity, both of which must be found within, or overlap, a closed wind circulation at 850 hPa. To be clear, for genesis to be counted as occurring at 1800 UTC 24 August, these characteristics must be present at that time. The genesis criteria from Snyder et al. (2010) are similar, but include a warm core as a threshold because it is necessary when using a lower resolution ensemble.

Compared with the GEFS, the CNTL predicts a similar mean track and track spread (figure not shown). However, while the GEFS produces poor forecasts for the genesis of Ernesto at 1 day of lead time (from 0000 UTC 24 August 2006), with 4 of its 14 members producing a tropical depression (Snyder et al. 2010), the CNTL predicts Ernesto's genesis in most of its 14 members, with 8 of the 14 reproducing a tropical depression. Overall, the CNTL produces several forecasts of a well-organized TC, whereas the large-scale GEFS fails to do so (Snyder et al. 2010). Clearly, the high-resolution regional forecasts improve the predictability of Ernesto's genesis by increasing the probability of forecast genesis.

Figure 4 displays the vorticity, wind vectors, and geopotential height at 850 hPa for each of the members in the CNTL at 1800 UTC 24 August, which is when the actual Ernesto reaches tropical depression (TD) status. First, it is evident how intense the forecast of the disturbance already is in many members by this time. Meanwhile, there is notable spatial variability among the members in terms of the circulation, geopotential height and vorticity. Thus, the CNTL not only produces forecasts of Ernesto's genesis by the best track genesis time, but also conveys the large amount of uncertainty inherent in large-scale GEFS forecasts.

Next, the differences between the CNTL and other bred vector-based ensemble forecasts are examined. Figure 5 presents the same synoptic view of FNLq3 at 1800 UTC 24

August. FNLq3 is the ensemble forecast in which the water vapor is bred every 3 h and forms the sole perturbations for all 14 members. We find that the majority of members predict well-organized vorticity maxima and fairly symmetric circulation patterns. Most of the disturbances in Figure 5 are less intense than those in the CNTL (Figure 4) and in general appear to be just above the threshold of tropical depression status. The breeding and perturbing of water vapor by itself appears to have decreased the amount of spread between the ensemble members compared with the CNTL.

Figure 6 illustrates the same synoptic map of the FNLth3 ensemble forecast at 1800 UTC 24 August. Note that the simulated TC-related circulations and vorticity are consistently more intense than those of the FNLq3 and many appear better organized than those in corresponding members in the CNTL. Similar to the FNLq3, the intensity variability is fairly small among the members in the FNLth3 and this result again characterizes the impact of perturbing just  $\theta$  (in FNLth3) compared with an ensemble with many perturbed variables (CNTL). The members of CNTL and FNLth3 show notably stronger TC genesis structures than those in FNLq3, which may be related to the fact that the average 850 hPa water vapor at the initial time in the latter ensemble experiments is notably reduced compared to those that did not breed the vapor (Figure 2).

The corresponding results obtained from the ensemble forecasts that bred the wind components (FNLuv3) are displayed in Figure 7. Note that the simulated TC circulations are consistently more intense than those of the FNLq3 and FNLth3 ensembles. Also, perturbing only the wind field does not produce significant spatial variability among the ensemble members, let alone intensity variability.

Figure 8 shows the ensemble forecasts (FNLuvqt3) from initial conditions that perturbed all variables, namely,  $\theta$ ,  $q$ ,  $u$  and  $v$  in 3-hourly breeding cycles. The forecasts produce disturbances that are weaker than the FNLq3 ensemble (Figure 5) and notably weaker than the FNLth3 ensemble (Figure 6). As a result, the genesis probability in FNLuvqt3 is lower than those in FNLq3 and FNLth3. However, compared with all mentioned ensemble experiments (FNLq3, FNLth3 and FNLuv3), FNLuvqt3 provides more variability in terms of both intensity and track in the forecasts. Therefore, it gives better representation of the uncertainties in terms of the environmental conditions, intensity and track of the disturbance at the time, compared with the ensembles that perturbed a single variable (FNLq3, FNLth3 and FNLuv3).

Similar to FNLuvqt3, ensemble results from all other experiments, FNLuvqt6, FNLuvqt12, and FNLuvqt3\_GEFS-BCs produce similar ensemble forecast spreads, although varying cycling periods and boundary conditions all exert impacts on the ensemble forecasts in terms of developing and non-developing cases and their environments. In addition, FNLq3\_height and GEFSth3 provide unique forecast biases, spreads, and TC statistics, and, considering all these

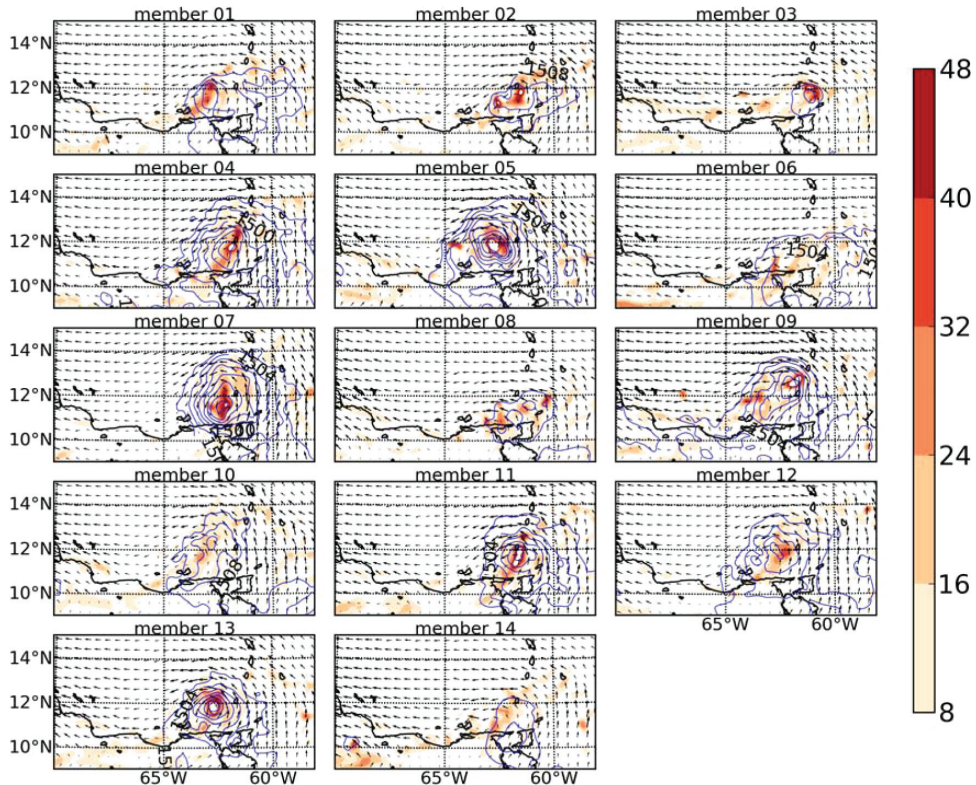


FIG. 4. Vorticity (shaded; unit:  $10^{-5} \text{ s}^{-1}$ ) and geopotential height (contours; 4 m intervals) of CNTL ensemble members at 850 hPa at 1800 UTC 24 August 2006.

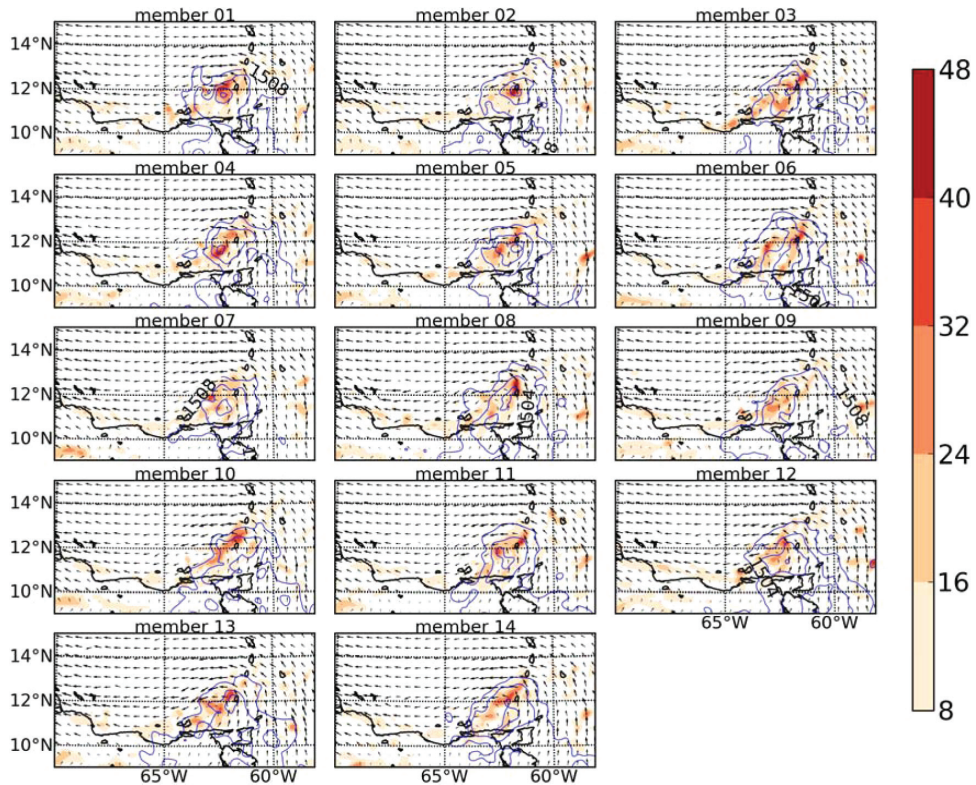


FIG. 5. Same as Figure 4, except for FNLq3.

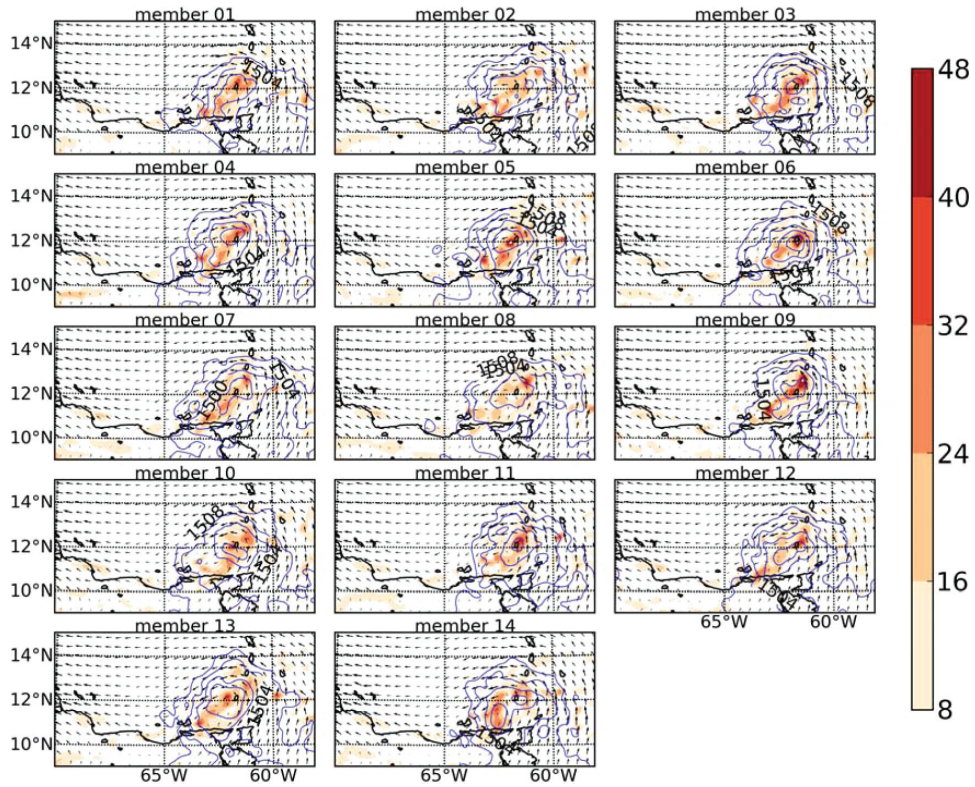


FIG. 6. Same as Figure 4, except for FNLth3.

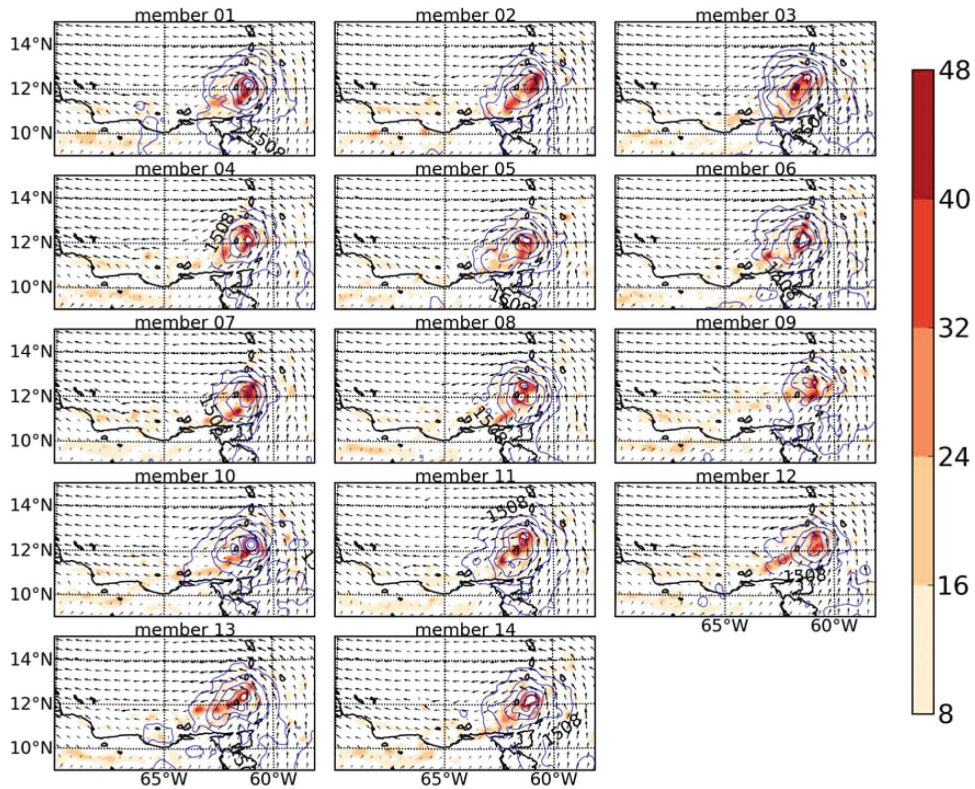


FIG. 7. Same as Figure 4, except for FNLuv3.

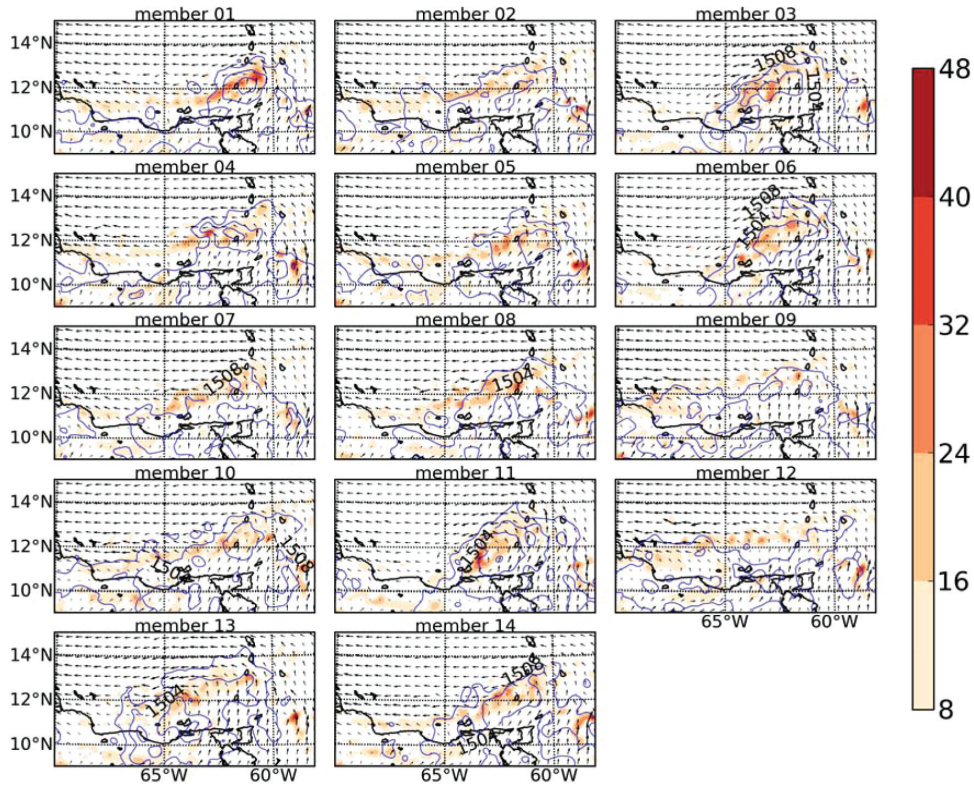


FIG. 8. Same as Figure 4, except for FNLuvqt3.

experiments in aggregate, we achieve a large sample with which to study the important environmental precursors in ensemble forecasts of Hurricane Ernesto’s genesis.

The statistics of forecasted genesis from different experiments are summarized in Table 2. It is clear that the distribution of genesis probability is uneven in different experiments. Specifically, genesis probabilities in experiments FNLth3 and FNLuv3 are higher than those in other experiments. The higher genesis probabilities are associated with the intense and more organized vorticity and circulation structure (Figures 6 and 7), as mentioned above. Overall, among the 140 total ensemble members in the various forecasts, we obtain 51 developing cases that predict Ernesto’s genesis, and 89 (non-developing) cases that fail predict Ernesto’s genesis. By contrasting the developing versus non-developing cases in this set of ensemble forecasts, we can evaluate the environmental precursors that effect Ernesto’s genesis on a statistical basis.

**4. Relative operating characteristics (ROC)**

We use relative operating characteristics (ROC) to evaluate the effect of a certain value (threshold) of vertical wind shear, water vapor or other metric on TC genesis likelihood. The ROC is a powerful way to verify the predictive power of various environmental thresholds. Specifically, these categorical forecasts from ensemble forecast thresh-

olds and the subsequent TC outcomes will produce “hit rate” and “false alarm rate” values to be entered into the ROC diagram (e.g., Figure 9), with false alarm rate on the x-axis and hit rate on the y-axis. The upper left corner of the ROC diagram represents a perfect forecast system (no false alarms, only hits). The closer any verification is to this upper left corner, the higher the predictive skill. The lower left corner (no hits or false alarms) represents a system, that never warns of an event. The upper right corner represents a system that is always warning for an event (see Figure 9).

To evaluate the relationship between precursors and the subsequent forecast of Ernesto’s genesis, the ROC diagrams are created by entering the fraction of true positives out of the positive genesis cases, versus the fraction of false positives out of the number of negative (or null) genesis members. The members are binned in each category depending on their initial values (at 0000 UTC 24 August 2006) of a particular field relative to the threshold of choice for that field, and depending on whether the same member subsequently predicts genesis at 1800 UTC 24 August 2006. A contingency table is created by using incremental thresholds of the chosen environmental data and seeing whether genesis, in the members corresponding to those particular thresholds, occurs or not. By way of plot orientation, a perfect predictive factor would result in a point in the upper left-hand corner, representing no false negatives

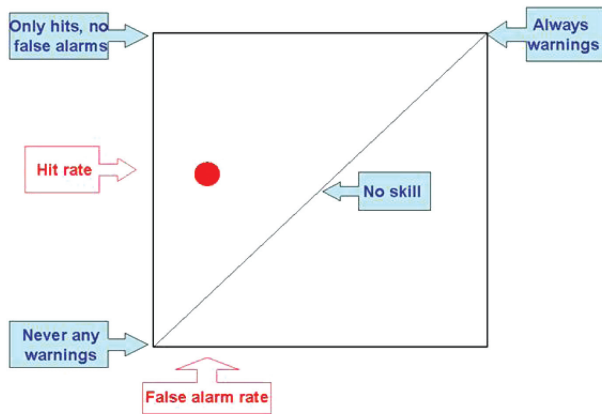


**FIG. 9.** The principle of the ROC diagram: a large number of probability forecasts are turned into categorical forecasts depending on whether the probability values of individual forecasts are above or below a certain threshold. The false alarm rate and the hit rate are calculated, thus determining the position in the diagram (red filled circle).

and no false positives. By contrast, perfectly random data, or data in which there is no predictive power, will lead to a “no-discrimination” line that runs diagonally from the bottom left to the top right corner.

The area under the ROC curve and above the no-discrimination line is indicative of positive predictive power. While negative relationships would naturally fall in the area below the no-discrimination line, in this study we will use only the area above the line so that the meaning of the statistics will be easier to decipher.

**5. Precursors of Ernesto’s genesis**

*a. Mid- to lower-level water vapor*

Because of its impact on convection, mid-to-lower-level water vapor is one of the most common environmental conditions that influence TC genesis (Bister and Emanuel 1997; Sippel and Zhang 2008). The concentration of near-TC moisture has long-been recognized as an important predecessor of genesis (Gray 1968). However, because

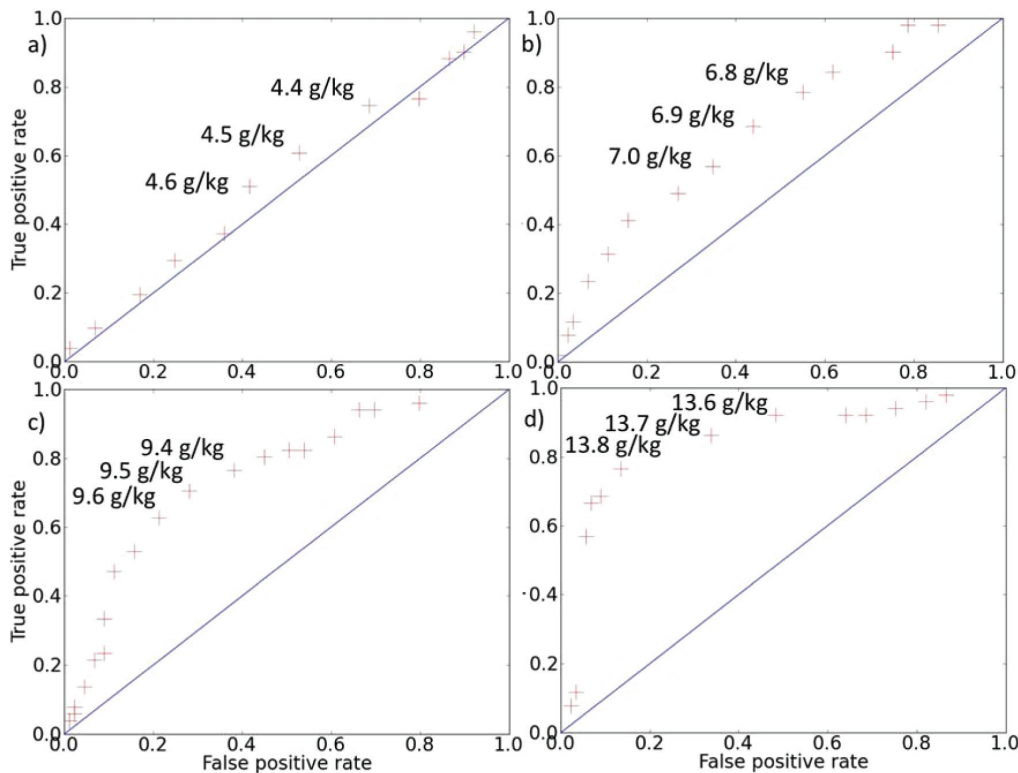


**FIG. 10.** Relative operating characteristic (ROC) curves showing relationship between genesis at 1800 UTC 24 August and average water vapor within a 100 km radius of simulated TC center at a) 500 hPa, b) 600 hPa, c) 700 hPa, and d) 850 hPa at 0000 UTC 24th August.

high water vapor is found extensively throughout the tropics, water vapor is seen as allowing rather than necessarily causing genesis to occur.

The four ROC plots in Figure 10 display the relationship between the TC genesis at 1800 UTC 24 August 2006 and average water vapor within 100 km radius from the center

of simulated pre-Ernesto disturbances at 500, 600, 700, and 850 hPa at 0000 UTC 24 August 2006. With a threshold increasing by 0.1 g/kg between 4.0 and 5.1 g/kg, it is apparent that the vapor at 500 hPa more often has a true positive rate than false positive rate. Namely, there is some positive predictive powers present here. At 600 hPa (Figure 3b), there is more positive area than there is at 500 hPa. The 700 hPa ROC figure shows even more positive area still, and finally at 850 hPa (Figure 3c,d), positive predictive power in terms of water vapor is maximized. The effect then declines in power below the 850hPa level (figures not shown). Overall, ROC curves at 700 and 850 hPa indicate quite an impressive relationship between water vapor within 100 km of the pre-Ernesto center and the prediction of TC genesis 18 h later. Further examination of the data behind Figure 3d shows that an area-averaged near-TC water vapor threshold of 13.8 g/kg at 850 hPa produces 39 true positive, 12 false positive, 12 false negative, and 77 true negative genesis cases 18 h later. Thus, with an initial water vapor threshold of 13.8 g/kg averaged over a 100km radius from the simulated pre-Ernesto's center, we are able to accurately predict 76 % of the genesis cases and 87 % of the null cases.

To illustrate how the water vapor differ for the developing versus non-developing cases, Figure 11 shows the water vapor composites for both genesis and nongenesis cases at the 500 and 600 hPa levels, and Figure 12 shows the 700 and 850 hPa levels. Note how water vapor is more associated with the easterly wave at 500-700 hPa, while it is much more locally distributed at 850 hPa. Compared to the differences between the genesis and nongenesis composites of water vapor at 500 hPa (Figure 4a), the genesis composite has roughly 0.3 g/kg more water vapor near the simulated pre-Ernesto's center and this difference extends for a few hundred square kilometers in all directions. Recall that at 500 hPa, a 0.3 g/kg difference in water vapor is not trivial. At 600 hPa (Figure 4b), the difference, between the composites, near the center of pre-Ernesto (notice the X) is now up to near 0.6 g/kg. Notice that in the center of the domain the genesis composite shows less water vapor than the nongenesis composite, due to the fact that the genesis cases tend to accompany a higher-amplitude wave, which produces a more southward extension of the midlevel dry tongue seen across the northern half of the domain. At 700 and 850 hPa (Figure 12), there is an anomalously high amount of water vapor for at least a 100 km radius from the center of pre-Ernesto in the genesis cases. At 850 hPa, the difference between the genesis versus nongenesis composites reaches 0.8 g/kg near the center. Thus, 18 h before genesis, greater water vapor in the environments throughout the lower half of the atmosphere, creates a notably higher chance of producing TC genesis.

#### b. Vertical wind shear

Vertical wind shear is calculated by the differences be-

tween vector winds at 200 hPa and at 850 hPa (Frank and Ritchie 2001; Knaff et al. 2004) within 500 km of radius from the simulated Ernesto's center. Figure 13 shows the ROC curves created by the relationship between vertical wind shear at 0000, 0300, and 0600 UTC 24 August against the genesis at 1800 UTC 24 August.

Vertical shear at the initial time is found to have a strong negative impact on the genesis 18 h later (Figure 13a), consistent with the common knowledge that small vertical wind shear provides more favorable conditions for TC genesis. Note that the effect of shear at 0300 UTC is greater than that at 0000 UTC (Figure 13). Using a threshold of 7.0 m/s vertical wind shear at 0300 UTC leads to 35 true positive, 23 false positive, 16 false negative, and 66 true negative genesis predictions. Of the 89 null cases, 66 (or 74 %) are predicted; of the 51 genesis cases, 35 (or 69%) are correctly predicted. The ROC curve appears very near the no-value diagonal line at 0600 UTC (Figure 14c). Tropical cyclone circulation often creates its own shear due to the fact that its upper-level anticyclonic flow accompanies a lower-level cyclonic flow. Because of the difficulty in identifying a complete vortex circulation before TC genesis, we are not able to remove the vortex circulation in the vertical wind shear calculations in the pre-genesis environment, and thus the mixed signal at 0600 UTC (Figure 13c) likely denotes that vertical shear accompanies the formation of Ernesto instead of necessarily inhibiting its formation.

#### c. Pre-existing vorticity

Contrary to water vapor and vertical shear, pre-existing vorticity maxima are often viewed as the impetus for genesis. There has been much discussion as to whether this pre-existing vorticity enables genesis mostly when it arises first in the middle or lower levels; these two scenarios are often described as a top-down (Bister and Emanuel 1997; Ritchie and Holland 1997; Simpson et al 1997) or bottom-up (Davis and Bosart 2001; Hendricks et al. 2004; Reasor et al. 2005; Montgomery et al. 2006) path to genesis, respectively. To evaluate the impact of pre-existing vorticity levels on forecasts of TC genesis, Figure 14 illustrates a ROC curve of the relationship between lower-level (800-900 hPa) and midlevel (500-600 hPa) vorticity at 0000 UTC 24 August and the TC genesis 18 h later. It is found that the lower-level vorticity has a weak, but positive genesis predictive power (Figure 14a). This power, or area under the curve, is not manifest at all thresholds, but occurs mostly at area-averaged values of  $7.5 \times 10^{-5}$  -  $9.0 \times 10^{-5} \text{ s}^{-1}$  over a 100 km radius from the simulated Ernesto center. Specifically, when a vorticity threshold of  $8.0 \times 10^{-5} \text{ s}^{-1}$  is applied, of the 51 cases in which genesis occurred, 37 (or 73%) are correctly predicted; of the 89 null cases, 37 (or 42 %) are predicted. The fact that we are able to accurately predict over 50 % of the genesis cases, while not dropping below 50 % in for the null cases, demonstrates the small but positive signal in the relationship between early low-level vorticity and Ernesto's genesis. This relationship,

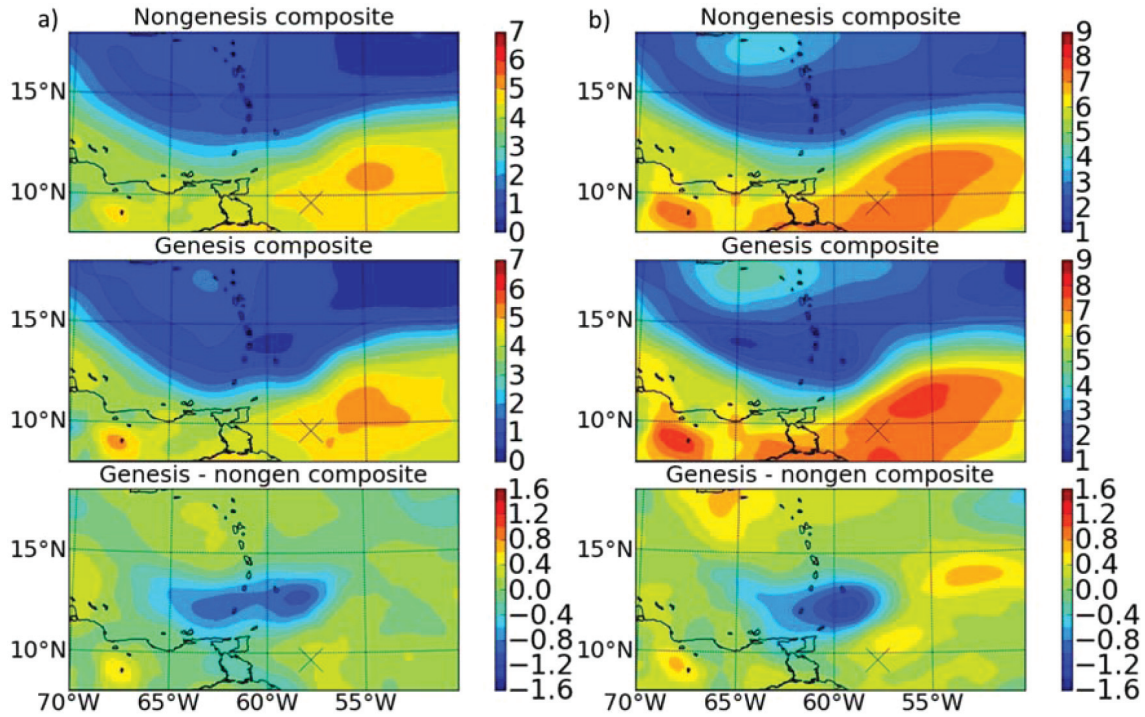


FIG. 11. Genesis and nongensis composites at 0000 UTC 24 August in terms of water vapor (g/kg) at a) 500 hPa and b) 600 hPa. X marks the location of the pre-Ernesto disturbance.

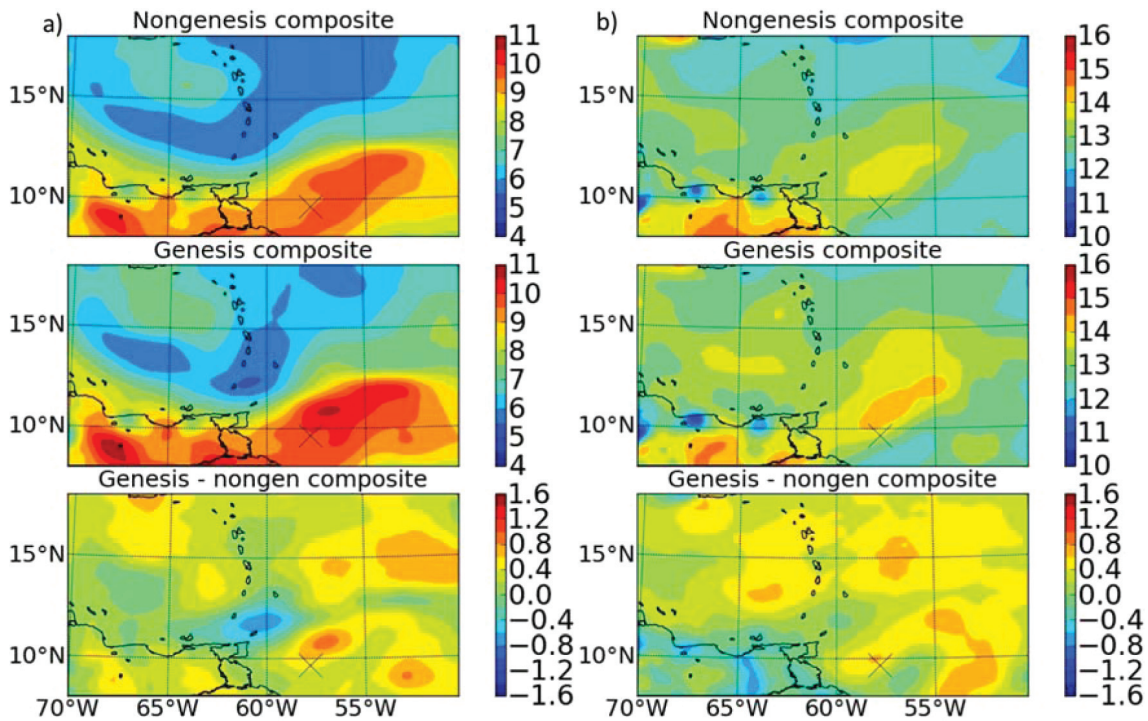


FIG. 12. Genesis and nongensis composites at 0000 UTC 24 August in terms of water vapor (g/kg) at a) 700 hPa and b) 850 hPa. X marks the location of the pre-Ernesto disturbance.

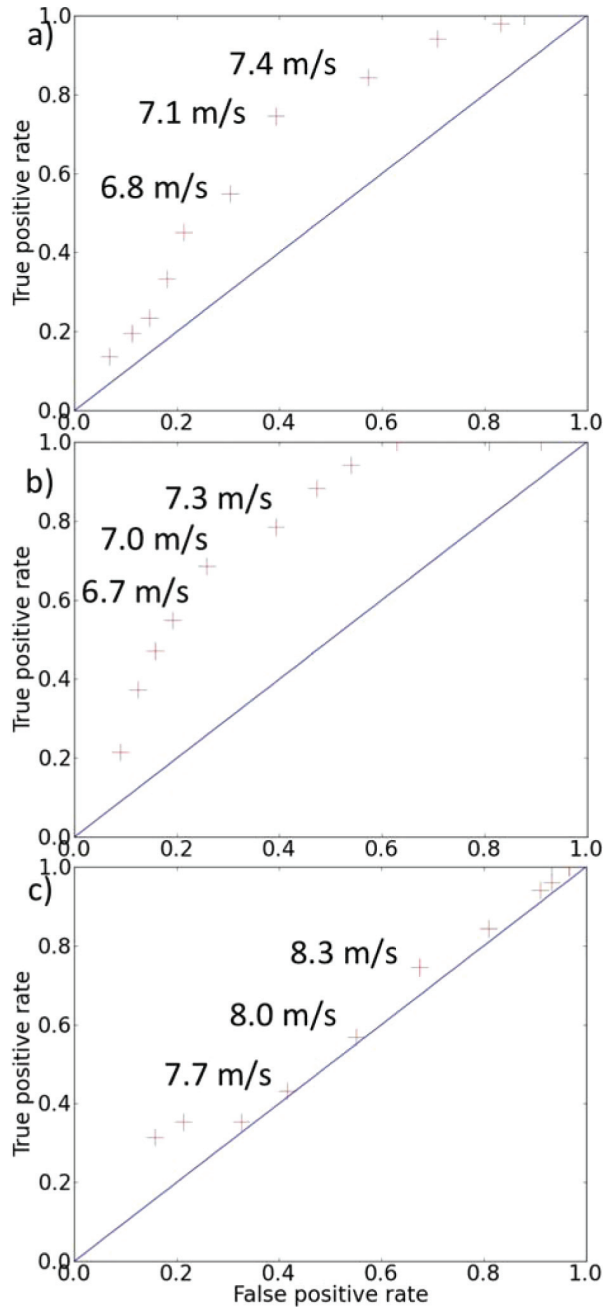


FIG. 13. ROC curves showing relationship between genesis at 1800 UTC 24 August and vertical shear within a 500 km radius of simulated TC center at a) 0000 UTC, b) 0300 UTC, and c) 0600 UTC 24 August 2006.

however, is notably weaker than that between genesis and either water vapor or vertical shear.

While initial lower-level vorticity is found to positively impact genesis, midlevel vorticity does not have such predictive power. As seen in Figure 14b, midlevel vorticity

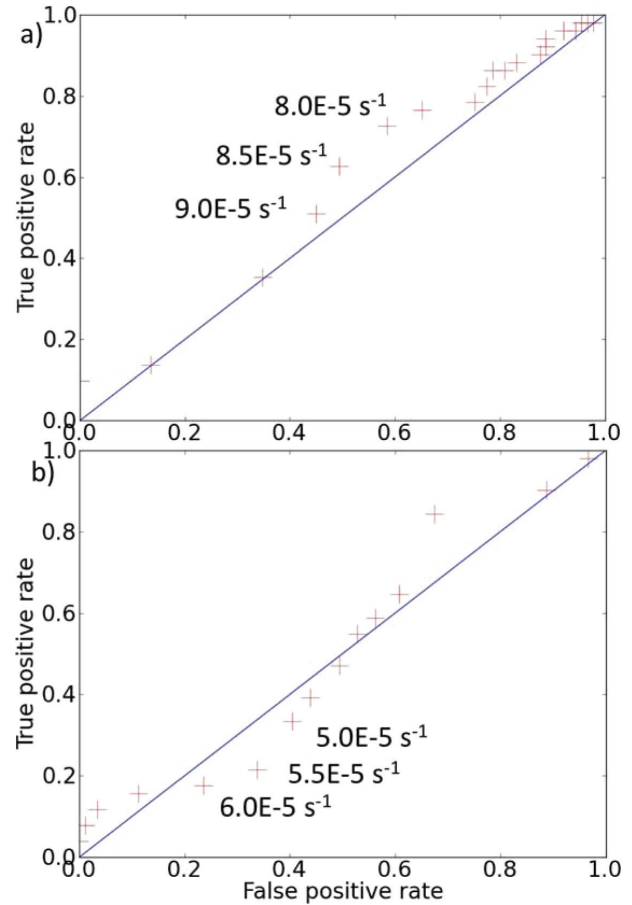


FIG. 14. ROC curves showing relationship between genesis at 1800 UTC 24 August and vorticity within a 100 km radius of simulated TC center a) from 800-900 hPa and b) from 500-600 hPa at 0000 UTC 24 August.

has a mixed if slightly negative relationship with genesis at 1800 UTC 24 August. While threshold vorticity values between  $1 \times 10^{-5} \text{ s}^{-1}$  and  $3.5 \times 10^{-5} \text{ s}^{-1}$  show a positive relationship with genesis, the correlation is negative when applying thresholds of  $4 \times 10^{-5} \text{ s}^{-1}$  and  $6.0 \times 10^{-5} \text{ s}^{-1}$ . Thus, the impact of midlevel vorticity on TC genesis appears to be unclear in our 140 members.

For further examination we break down the genesis and nongenesis cases into composites of both lower and midlevel vorticity in Figure 15. Figure 15a shows that the genesis cases start with a more notable vorticity maxima associated with the lower-level easterly wave. Because this lower-level wave is weaker in the nongenesis case, the magnitude of the vorticity over the inverted wave downstream is also weaker (Figure 15b). Since vorticity is negative in this down-stream portion of the wave, the nongenesis composite has smaller negative values than the genesis composite, thus leading to the negative difference values

directly south of the Lesser Antilles in Figure 15a. When examining the midlevel vorticity composites (Figure 15b), we notice that the maximum positive difference vorticity values are somewhat similar at this height, except the shift between the positive and negative difference values is now oriented in a north-south direction. These differences from

500 to 600 hPa, however, appear to be caused by the higher vorticity values in nongensis case from 58 to 60°W and between 12 and 13°N. Again, these vorticity differences at 500 to 600 hPa do not significantly affect genesis in a conclusive manner. Overall, while these midlevel results are difficult to decipher, those in the lower-levels show a clear,

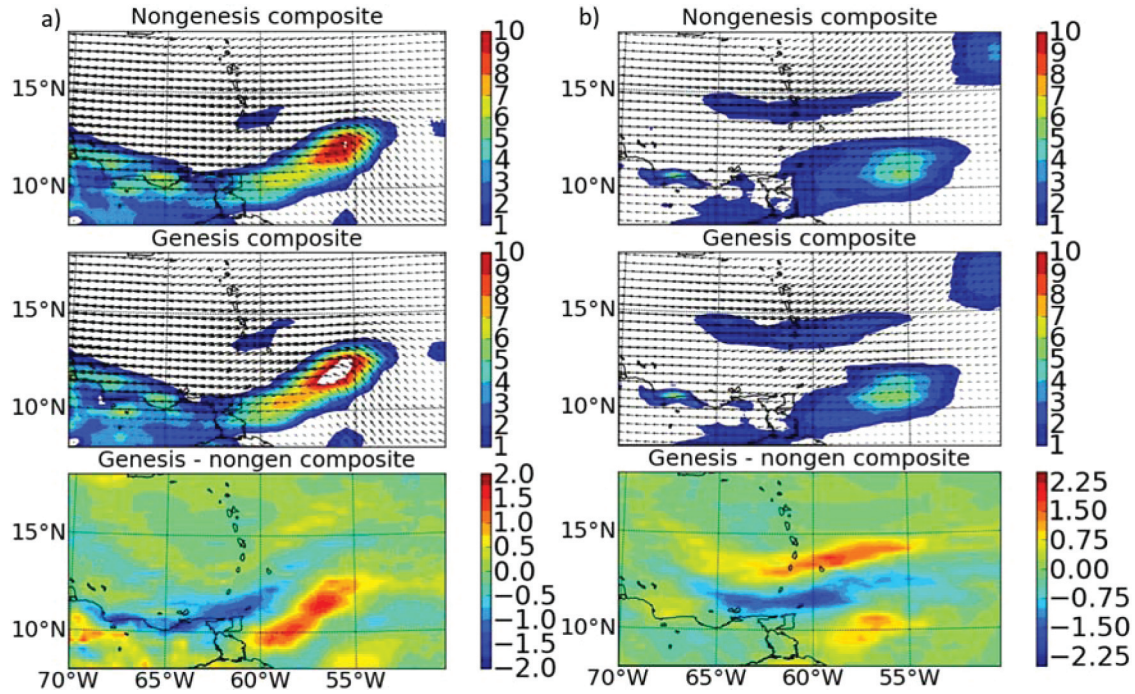


FIG. 15. Genesis and nongensis composites at 0000 UTC 24 August in terms of vorticity (s-1) and the wind field at a) 800-900 hPa and b) 500-600 hPa.

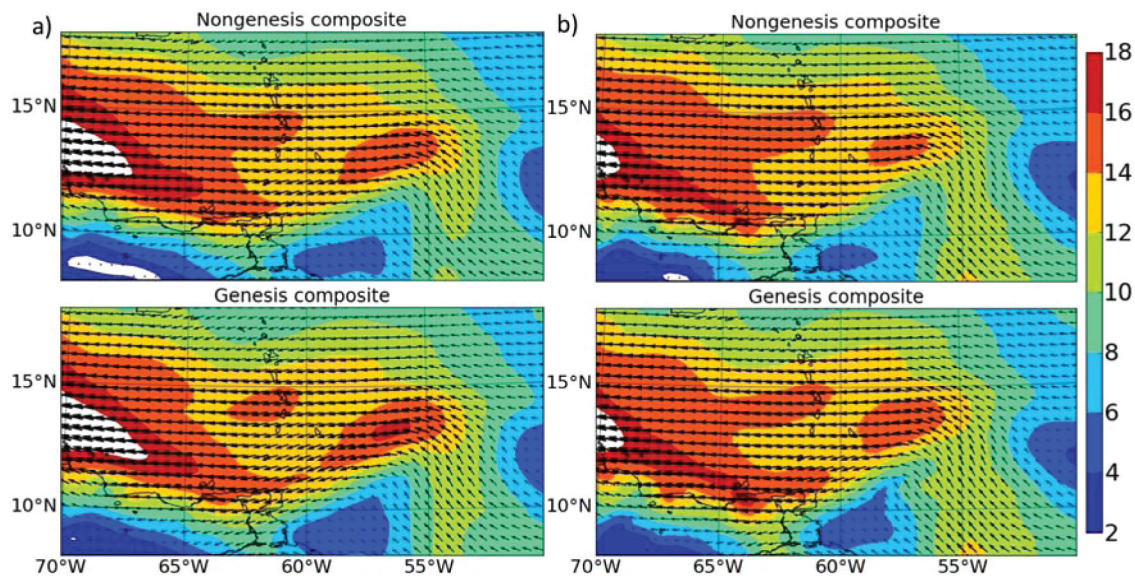


FIG. 16. Genesis and nongensis composites in terms of 850 hPa wind speed (m/s) and circulation at a) 0000 UTC and b) 0300 UTC 24 August.

positive relationship between vorticity and genesis.

*d. Wave strength*

In order to better describe the impact of the initial strength of the easterly wave on genesis 18 h later, 850 hPa winds for genesis and nongensis composites are calculated at 0000 and 0300 UTC 24 August and displayed in Figure 16. In these four subfigures, the easterly wave is positioned around 57°W and 12°N. First, at 0000 UTC, the wave has a much more developed circulation in the genesis composite than in the nongensis composite. Specifically, in the nongensis composite at this time, a northerly component of the wind on the downwind side of the wave axis is conspicuously absent. In the genesis cases, winds around 58°W and 13°N (i.e., in the downwind section) are 2-4 m/s stronger and have much more of a northerly (i.e., vertical) component compared with the nongensis members. These directional differences are even more prominent at 0300 UTC (Figure 16 b). Recall that the impacts of these differences are reflected in the genesis result 15-18 h later, despite the other complicated environmental factors present. While the genesis process is often seen as stochastic even in the presence of a pre-existing wave (Simpson et al. 1997; Reasor et al. 2005), in this study, we find that TC genesis likelihood is very much related to the strength of the pre-existing low-level wave up to 18 h before genesis. The statistical significance of these calculations will be discussed below.

*e. Upper-level warmth*

With large number of ensembles forecasting the genesis of Hurricane Ernesto (2006), we will also determine the relationship, if any, between initial core potential temperature and genesis at 1800 UTC 24 August. ROC curves are calculated for 200 to 500 hPa  $\theta$  within 100 km of the simulated pre-Ernesto center at 0000 and 0300 UTC 24 August in Figure 17. We find that initial upper-level  $\theta$  values at 0000 UTC do not have a significant impact on genesis (Figure 17a). However, moving forward 3 h to the simulation

at 0300 UTC, the situation changes significantly. In Figure 17b, the effect of upper-level  $\theta$  on genesis is positive and consistent across various core  $\theta$  thresholds. This is surprise, as there is only a slight difference in upper-level warmth between the genesis and non-genesis cases; in addition, we do not expect notable warm cores to be present 15 h before best track genesis. Zhang and Zhu (2012) recently pointed out that upper-level warmth results in significant surface sea level pressure decrease during TC genesis and rapid intensification and this may relate to what we are seeing in our ROC diagrams (Figure 17).

In order to view the extent of these initial warm cores and how they vary between the genesis and nongensis cases, the two corresponding composites are created and presented in Figure 18. We see that at the initial time (Figure 18a), the upper-level  $\theta$  in the genesis composite is only slightly warmer (i.e., 0.1K) than that in the nongensis composite. Three hours later, however, the genesis composite shows values around 1.0 K greater than in the nongensis composite in the pregenesis region, southeast of the Lesser Antilles. The warm core is present quite early in the

**TABLE 3.** P-values from the Kolmogorov-Smirnov test performed between genesis and nongensis composites of various parameters in ensemble groupings

Field	Median	0-9
Shear 00UTC	.11	.00
Shear 03UTC	.05	.00
Shear 06UTC	.10	.29
Vapor 500hPa	.13	.82
Vapor 600hPa	.14	.01
Vapor 700hPa	.24	.00
Vapor 850hPa	.05	.00
Vorticity mid-level	.06	.16
Vorticity low-level	.07	.22

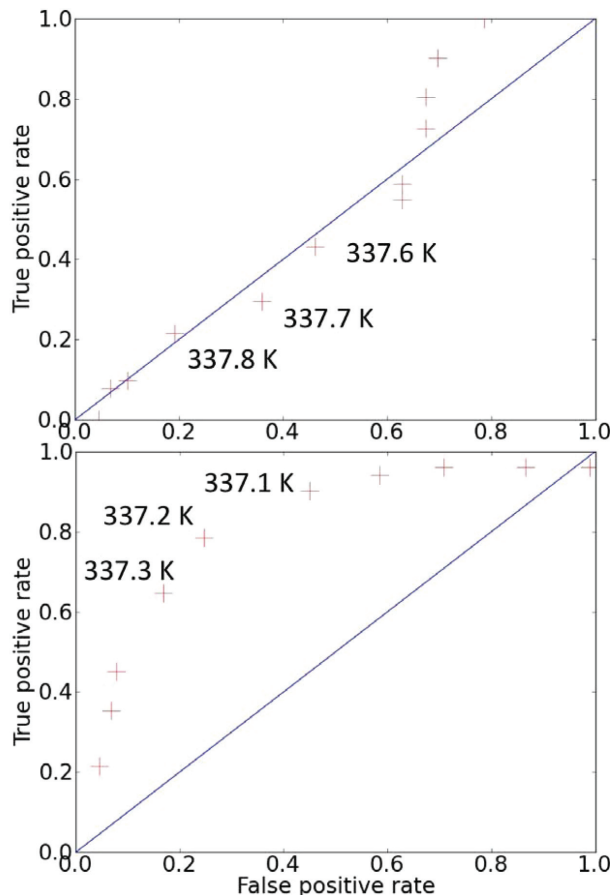


**FIG. 17.** ROC curves showing relationship between genesis at 1800 UTC 24 August and theta within a 100 km radius of simulated TC center from 200-500 hPa at a) 0000 and b) 0300 UTC 24 August.

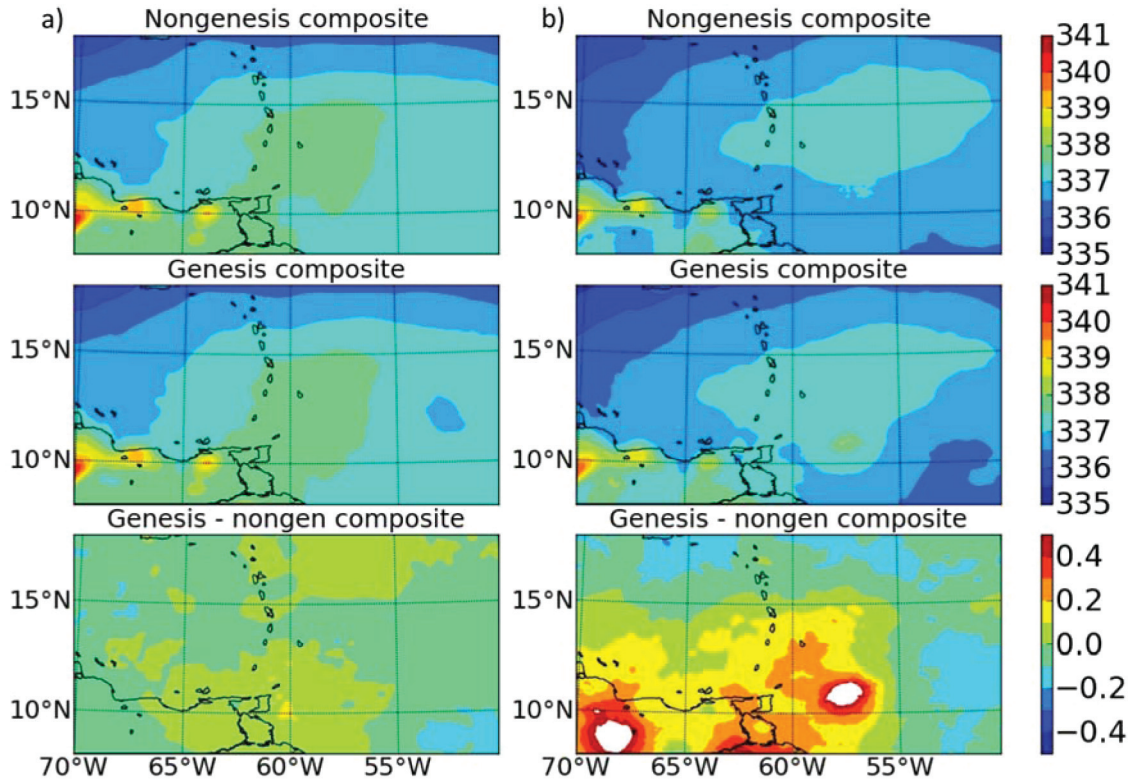


FIG. 18. Genesis and nongensis composites in terms of theta (K) from 200 to 500 hPa at a) 0000 UTC and b) 0300 UTC 24 August.

simulation as this is 15 h *before* the disturbance becomes a TD. Many of the members possess genesis-like characteristics long before genesis.

#### f. Statistical significance of the results

In order to investigate the statistical significance of the relationships enumerated above, a Kolmogorov-Smirnov (KS) two-sample test is conducted. This nonparametric test provides a p-value, which describes the odds of the two samples being drawn from the same continuous distribution. A lower p-value means a higher statistical significance. In order to account for the fact that the 10 experiments using 140 ensemble members may actually represent many fewer degrees of freedom in a particular field, we split the sample into groups of two ensemble experiments (20 members) each, using each of 45 possible combinations, and determine the p-value for the particular genesis precursor relationship in each of these smaller groupings. Table 3 shows the results of the KS test on several of the aforementioned environmental precursors, using the corresponding genesis and nongensis composites over all ensemble members. This is presented in terms of the median value from the aforementioned two-ensemble groupings and also the KS test performed over all 10 ensemble experiments.

We first look at the impact of water vapor on Ernesto's genesis at 1800 UTC 24 August. In the important layers of 700 and 850 hPa, the chances are effectively 0 that the composites of genesis and nongensis cases are from the same distribution based on the calculation performed over the entire 10 ensemble experiments. In checking the robustness of the results, we find that for small samples of two ensemble experiments, the median p-value is 0.05 at 850 hPa. For water vapor at 600 and 700 hPa, the p-values of the combined 10 ensemble experiments are also below 0.05, while the two-ensemble median p-values are notably higher at 600 and 700 hPa than at 850 hPa. Overall this confirms what is found in the ROC statistics, in which the largest explanatory power between genesis and initial water vapor also occurs at 850 hPa (Figure 10).

In terms of the impact of vertical shear on genesis, the KS statistics also confirm what is found in the ROC curves (Figure 13). Specifically, the KS test calculated over the 10 ensemble experiments yields p-values less than 0.05 at 0000 and 0300 UTC, but not at 0600 UTC. Considering the robustness of the difference between the genesis and non-genesis shear profiles at 0300 UTC, we find that the median p-value of two-ensemble experiments reaches the common 0.05 alpha threshold. While the ROC genesis predictive power is greater for water vapor at 850 hPa at 0000

UTC than for vertical shear at 0300 UTC, the statistical significance of the two relationships is quite similar (Table 3). We suspect that shear values at 0300 UTC rather than 0000 UTC are more important to genesis because several ensembles' wind fields are not perturbed directly at 0000 UTC and are only differentiated among the members, 3 h later, by the original perturbations of vapor or  $\theta$ . It is likely that the wind perturbations have adjusted according to the thermal fields in the simulation at 3 h and then start taking the effects to the genesis. Vertical shear in the simulation at 6 h appears to decline in its importance to genesis, since the median p-value increases to 0.10 and the overall KS p-value increases to 0.29, and the explanatory power in the ROC figure decreases compared to 0300 UTC as well (Figure 13).

## 6. Concluding remarks

In this paper, we first generate a set of high-resolution regional ensemble forecasts with a bred vector method. Then we use this set of 140 ensemble members to study the environmental precursors for Hurricane Ernesto's genesis by contrasting the genesis and nongensis (e.g., developing and non-developing) cases. Specifically, ROC curves, composite figures, and the Kolmogorov-Smirnov test are applied to characterize the relationship between important environmental parameters near the beginning of the simulation and genesis likelihood 15-18 h later. Individually, 850 hPa water vapor, vertical wind shear, the strength of the 850 hPa pre-existing wave and upper-level warming provide notable predictive power for Ernesto's genesis.

Despite the fact that background moisture is quite high in the tropics in August, we find that moisture values near the center of a TC disturbance play an important role in determining whether a pre-existing disturbance will develop into an organized TC. For example, solely by using the criterion of an area averaged water vapor threshold of 13.8 g/kg at 850 hPa around the pre-existing disturbance, we are able to successfully predict 76% of the genesis cases that occurred and 87% of the null cases. The impact of initial water vapor at 700 and 600 hPa on subsequent genesis is slightly less strong, but still significant, nevertheless.

Vertical wind shear is another important parameter related to genesis. In this study, we find that 200-850 hPa vertical wind shear within 500 km of the nascent TC center has a statistically significant relationship to genesis 15-18 h later. Using a vertical shear threshold of 7.0 m/s at 0300 UTC, we are able to successfully predict 69 % of the genesis cases and 74 % of the null cases.

Of all the easterly waves that come from Africa each summer and fall, the number that leads to TC formation is quite small. Among 140 ensemble members in this study, the strength of the 850 hPa pre-existing wave differs considerably between composites of the genesis and nongensis cases. Vorticity values at 800-900 and 500-600 hPa have a more complicated relationship with genesis and no conclusive statistics are obtained. Nevertheless, composite

figures lead us to believe that low-level initial vorticity played a larger role in Ernesto's ultimate genesis than did mid-level vorticity.

Despite the large number of resolved and unresolved processes ultimately affecting TC formation, the pre-existing environmental conditions played a significant role in the TC genesis process of Hurricane Ernesto. While these results have been derived from a case study, we have used genesis/nongensis composites, ROC curves, and bootstrapped Kolmogorov tests to demonstrate the importance of various pre-genesis environmental fields to the likelihood of subsequent TC formation. The variance in pre-existing vorticity, moisture, and vertical shear among many ensemble members leads to a better understanding of the impact of environmental precursors on Ernesto's genesis. The methodologies used in this study can also be applied to many other TC cases. However, slightly different factors influence TC genesis in various basins, in different seasons, and even in various parts of the Atlantic Ocean. Such differences may result in notable variations from the statistics in this paper. In addition, there might be limitations in the use of the breeding method to study tropical dynamics in areas where moist convection dominates (Cheung 2001). Therefore, a larger sample of TC cases from several basins and different times of the year as well as more sophisticated ensemble systems would help better establish the nature of the relationships between precursors and TC genesis in future work. Furthermore, it would also be useful to evaluate the physical processes associated with TC genesis and the related predictability with ensemble forecasting.

## Acknowledgements

The authors greatly appreciate Drs. Carolyn Reynolds from the Naval Research Laboratory and Jeffrey Anderson from NCAR for their useful comments for this study. This study is supported by research grant from the Office of Naval Research (ONR) through award numbers N000140810308 and N000141310582.

We also thank the NCAR WRF model development group for their efforts in developing the community model. The Center for High Performance Computing (CHPC) at the University of Utah provided computing support for this study.

## References

- Aberson, S. D., 2001: The ensemble of tropical cyclone track forecasting models in the North Atlantic basin (1976-2000). *Bull. Amer. Meteor. Soc.*, **82**, 1895-1904.
- Bister, M., and K. A. Emanuel, 1997: The genesis of Hurricane Guillermo: TEXMEX analyses and a modeling study. *Mon. Wea. Rev.*, **125**, 2662-2682.
- Buizza, R., M. Miller, and T. N. Palmer, 1999: Stochastic representation of model uncertainties in the ECMWF ensemble prediction system. *Quart. J. Roy. Meteor. Soc.*, **125**, 2887-2908.
- Chen, S.-H., and W.-Y. Sun, 2002: A one-dimensional time dependent cloud model. *J. Meteor. Soc. Japan*, **80**, 99-118.

- Chen, S. S., and W. M. Frank, 1993: A numerical study of the genesis of extratropical convective mesovortices. Part I: Evolution and dynamics. *J. Atmos. Sci.*, **50**, 2401-2426.
- Cheung, K. K. W., 2001: Ensemble forecasting of tropical cyclone motion: Comparison between regional bred modes and random perturbations. *Meteor. Atmos. Phys.*, **78**, 23-34.
- Cheung, K. K. W., and R. L. Elsberry, 2002: Tropical cyclone formations over the western north Pacific in the Navy Operational Global Atmospheric Prediction System forecasts. *Wea. Forecasting*, **17**, 800-820.
- Davis, C. A., and L. F. Bosart, 2001: Numerical simulations of the genesis of Hurricane Diana (1984). Part I: Control simulation. *Mon. Wea. Rev.*, **129**, 1859-1881.
- Dudhia, J., 1989: Numerical study of convection observed during the Winter Monsoon Experiment using a mesoscale two-dimensional model. *J. Atmos. Sci.*, **46**, 3077-3107.
- Dunkerton, T. J., M. T. Montgomery, and Z. Wang, 2009: Tropical cyclogenesis in a tropical wave critical layer: Easterly waves. *Atmos. Chem. Phys.*, **9**, 5587-5646.
- Frank, W. M., and E. A., Ritchie, 2001: Effects of vertical wind shear on the intensity and structure of numerically simulated hurricanes. *Mon. Wea. Rev.*, **129**, 2249-2269.
- Gall R., J. Franklin, F. Marks, E. N. Rappaport, and F. Toepfer, 2013: The hurricane forecast improvement project., *Bull. Amer. Meteor. Soc.*, **94**, 329-343.
- Gray, W. M., 1968: Global view of the origin of tropical disturbances and storms. *Mon. Wea. Rev.*, **96**, 969-700.
- Grell, G. A. and D. Devenyi, 2002: A generalized approach to parameterizing convection combining ensemble and data assimilation techniques. *Geoph. Res. Lett.*, **29**, NO 14., 10.1029/2002GL015311, 2002.
- Hendricks, E. A., M. T. Montgomery, and C. A. Davis, 2004: The role of "vortical" hot towers in the formation of Tropical Cyclone Diana (1984). *J. Atmos. Sci.*, **61**, 1209-1232.
- Hennon, C. C., and J. S. Hobgood, 2003: Forecasting tropical cyclogenesis over the Atlantic basin using large-scale data. *Mon. Wea. Rev.*, **131**, 2927-2940.
- Hong, S. Y., Y. Noh, and J. Dudhia, 2006: A new vertical diffusion package with an explicit treatment of entrainment processes. *Mon. Wea. Rev.*, **134**, 2318-2341.
- Kerns, B., K. Greene, and E. Zipser, 2008: Four years of tropical ERA-40 vorticity maxima tracks. Part I: Climatology and vertical vorticity structure. *Mon. Wea. Rev.*, **136**, 4301-4319.
- Knaff, J. A., S. A. Seseske, M. DeMaria, and J. L. Demuth, 2004: On the influences of vertical wind shear on symmetric tropical cyclone structure derived from AMSU. *Mon. Wea. Rev.*, **132**, 2503-2510.
- Liu, H., J. Anderson, Y.-H. Kuo, 2012: Improved analyses and forecasts of Hurricane Ernesto's genesis using radio occultation data in an ensemble filter assimilation system. *Mon. Wea. Rev.*, **140**, 151-166.
- McBride, J. L., and R. Zehr, 1981: Observational analysis of tropical cyclone formation. Part II: Comparison of non-developing versus developing storms. *J. Atmos. Sci.*, **38**, 1132-1151.
- McLay, J. G., C. H. Bishop, and C. A. Reynolds, 2008: Evaluation of the ensemble transform analysis perturbation scheme at NRL. *Mon. Wea. Rev.*, **136**, 1093-1108.
- Mlawer, E. J., S. J. Taubman, P. D. Brown, M. J. Iacono, and S. A. Clough, 1997: Radiative transfer for inhomogeneous atmosphere: RRTM, a validated correlated-k model for the long-wave. *J. Geophys. Res.*, **102**, 16 663-16 682.
- Montgomery, M. T., and J. Enagonio, 1998: Tropical cyclogenesis via convectively forced vortex Rossby waves in a three-dimensional quasigeostrophic model. *J. Atmos. Sci.*, **55**, 3176-3207.
- , M. E. Nicholls, T. A. Cram, and A. B. Saunders, 2006: A vortical hot tower route to tropical cyclogenesis. *J. Atmos. Sci.*, **63**, 355-386.
- , Z. Wang, and T. J. Dunkerton, 2010: Coarse, intermediate and high resolution numerical simulations of the transition of a tropical wave critical layer to a tropical storm. *Atmos. Chem and Phys.*, **10**, 10803-10827.
- Nolan, D. S., E. D. Rappin, and K. A. Emanuel, 2007: Tropical cyclogenesis sensitivity to environmental parameters in radiative-convective equilibrium. *Quart. J. Roy. Meteor. Soc.*, **133**, 2085-2107.
- Reasor P. D., Montgomery M. T., Bosart L. F. 2005. Mesoscale observations of the genesis of Hurricane Dolly (1996). *J. Atmos. Sci.*, **62**, 3151 - 3171.
- Reynolds, C. A., J. Teixeira, and J. G. McLay, 2008: Impact of stochastic convection on the ensemble transform. *Mon. Wea. Rev.*, **136**, 4517-4526.
- Ritchie, E. A., and G. J. Holland, 1997: Scale interactions during the formation of Typhoon Irving. *Mon. Wea. Rev.*, **125**, 1377-1396.
- Rogers, R., S. Aberson, M. Black, P. Black, J. Cione, P. Dodge, J. Dunion, J. Gamache, J. Kaplan, M. Powell, N. Shay, N. Surgi, and E. Uhlhorn, 2006: The Intensity Forecasting Experiment: A NOAA multiyear field program for improving tropical cyclone intensity forecasts. *B. Am. Meteorol. Soc.*, **87**, 1523-1537.
- Simpson, J., E. Ritchie, G. J. Holland, J. Halverson, and S. Stewart, 1997: Mesoscale interactions in tropical cyclone genesis. *Mon. Wea. Rev.*, **125**, 2643-2661.
- Sippel, J. A., and F. Zhang, 2008: A probabilistic analysis of the dynamics and predictability of tropical cyclogenesis. *J. Atmos. Sci.*, **65**, 3440-3459.
- Skammarock, W.C., J.B. Klemp, J. Dudhia, D.O. Gill, D.M. Barker, M.G. Duda, X.-Y. Huang, W. Wang, and J.G. Powers, 2008: A description of the Advanced Research WRF Version 3. NCAR Tech. Note NCAR/TN-475+STR., June 2008, 133 pp.
- Snyder, A., Z. Pu, and C.A. Reynolds, 2011: Impact of stochastic convection on ensemble forecasts of tropical cyclone development. *Mon. Wea. Rev.*, **139**, 620-626.
- Snyder, A., Z. Pu, and Y. Zhu, 2010: Tracking and verification of the east Atlantic tropical cyclone genesis in NCEP global ensemble: Case studies during NASA African monsoon multi-disciplinary analyses. *Wea. Forecasting*, **25**, 1397-1411.
- Toth, Z., and E. Kalnay, 1993: Ensemble forecasting at NMC: The generation of perturbations. *Bull. Amer. Meteor. Soc.*, **74**, 2317- 2330.
- , and E. Kalnay, 1997: Ensemble forecasting at NCEP and the breeding method. *Mon. Wea. Rev.*, **125**, 3297-3319.
- Wei, M., Z. Toth, R. Wobus, Y. Zhu, and C. H. Bishop, 2008: Initial perturbations based on the ensemble transform (ET) technique in the NCEP global operational forecast system. *Tellus*, **60A**, 62-79.
- Zhang, D.-L., and L. Zhu (2012), Roles of upper-level processes in tropical cyclogenesis, *Geophys. Res. Lett.*, **39**, L17804, doi:10.1029/2012GL053140.